

Thermodynamics of fluctuations based on time-and-space averagesJames E. McClure *Virginia Polytechnic Institute and State University, Blacksburg, Virginia 24061, USA*Steffen Berg *Shell Global Solutions International B.V., Grasweg 31, 1031HW Amsterdam, The Netherlands*Ryan T. Armstrong *School of Minerals and Energy Resources Engineering, University of New South Wales, Sydney 2052, Australia*

(Received 10 December 2020; revised 21 May 2021; accepted 23 June 2021; published 20 September 2021)

We develop nonequilibrium theory by using averages in time and space as a generalized way to upscale thermodynamics in nonergodic systems. The approach offers a classical perspective on the energy dynamics in fluctuating systems. The rate of entropy production is shown to be explicitly scale dependent when considered in this context. We show that while any stationary process can be represented as having zero entropy production, second law constraints due to the Clausius theorem are preserved due to the fact that heat and work are related based on conservation of energy. As a demonstration, we consider the energy dynamics for the Carnot cycle and for Maxwell's demon. We then consider nonstationary processes, applying time-and-space averages to characterize nonergodic effects in heterogeneous systems where energy barriers such as compositional gradients are present. We show that the derived theory can be used to understand the origins of anomalous diffusion phenomena in systems where Fick's law applies at small length scales, but not at large length scales. We further characterize fluctuations in capillary-dominated systems, which are nonstationary due to the irreversibility of cooperative events.

DOI: [10.1103/PhysRevE.104.035106](https://doi.org/10.1103/PhysRevE.104.035106)**I. INTRODUCTION**

The ergodic hypothesis is central to many results of statistical physics. The basic premise is that a system will explore all possible energetic microstates if considered over a sufficiently long interval of time. The concept of ergodicity is thereby linked with the mixing of information within a system [1]. Canonical proofs of the ergodic hypothesis rely on the equivalence of spatial, temporal, and ensemble averages in the limit of infinite time [2,3]. Scale considerations and the rate of mixing necessarily constrain the applicability of the ergodic hypothesis when considering finite regions of time, particularly for systems where mixing is slow compared to the physical timescale of interest [4]. Many physical systems are known to exhibit behavior that is inconsistent with the ergodic hypothesis. Well-known examples include anomalous diffusion in biological systems [5–7], glassy systems [8–10], capillary phenomena and nucleation [11–16], and granular systems where multiscale effects are present due to jamming and force chains [17–20]. A common element for these systems is that they involve spatially heterogeneous materials where available thermal energy is insufficient to overcome internal energy barriers. This inhibits mixing and prevents the system from exploring all possible microstates within the timescale of interest.

In this paper, we demonstrate that time-and-space averaging can be applied as a mechanism to mathematically mix

information at a desired scale, providing a natural path forward in systems where nonergodic effects are encountered. Multiscale fluctuation terms arise in the nonequilibrium description due to spatial and temporal deviations associated with intensive thermodynamic variables. Our approach is rooted in classical thermodynamics and offers a formally distinct perspective on fluctuations as compared to statistical theory, e.g., [21–27]. The presented methods can be a general tool for understanding how energy dynamics translate across length and time scales. First we consider a basic example, demonstrating that the Carnot cycle and Maxwell's demon can be interpreted in terms of energy fluctuations. Then we consider mass transport phenomena in the context where Fick's law applies at a small length scale but fails at larger scales. Finally, the approach will be applied to nonequilibrium behavior in multiphase systems, where fluctuations occur due to capillary effects and confinement [27]. How to characterize and interpret these fluctuations has been a longstanding problem for immiscible fluid flow in porous media, and has broad applications to other systems [26,28–36].

II. TIME-AND-SPACE AVERAGED THERMODYNAMICS

A classical thermodynamic description is defined by considering the internal energy to depend on the entropy S as well as other extensive physical properties of the system, X_i (e.g.,

volume, number of particles, etc.) [37–39],

$$U = U(S, X_1, X_2, \dots, X_n). \quad (1)$$

Intensive quantities are then defined according to Euler’s homogeneous function theorem,

$$T = \left(\frac{\partial U}{\partial S} \right)_{X_i}, \quad Y_i = \left(\frac{\partial U}{\partial X_i} \right)_{S, X_{j \neq i}}, \quad (2)$$

such that

$$U = TS + Y_i X_i \quad (3)$$

describes the internal energy of the system at equilibrium. In practice, measurements of thermodynamic quantities are always averages carried out over some finite region of space and time. The measurement timescale τ_m can be used to infer the size of the region where local equilibrium conditions exist. For example, if a thermometer is used to measure the temperature, any material that is close enough to the measurement point can be considered to be in local equilibrium with the measured value. Diffusive mechanisms are responsible for mixing energy within the system since it is the movement of the molecules and their interaction with each other that creates ergodic conditions. Given a fixed timescale τ_m , an associated length scale is obtained from the Einstein relation, which predicts the mean squared displacement (MSD) for molecular trajectories $x(t)$,

$$\int_0^{\tau_m} x^2(t) dt \sim D\tau_m, \quad (4)$$

where D is the diffusion coefficient. Since MSD predicts the average distance that molecules drift within time τ_m , the system is locally well mixed at that length scale. Ergodic behavior should therefore be observed within a surrounding spherical region with volume

$$\mathcal{V} \leq \frac{4\pi}{3} (D\tau_m)^{3/2}. \quad (5)$$

During the elapsed time τ_m , molecules will explore a spatial region with size \mathcal{V} such that spatial, temporal, and ensemble averages are interchangeable at this scale. Smaller \mathcal{V} can be chosen as long as the defined region is larger than the molecular length scale. At the scale of \mathcal{V} , the theoretical bridge between the molecular and hydrodynamic description can be provided by statistical theory, relying on the validity of the ergodic hypothesis [40]. Equation (3) can then be rescaled to treat extensive measures on a per-unit-volume basis,

$$\frac{U}{\mathcal{V}} = T \frac{S}{\mathcal{V}} + Y_i \frac{X_i}{\mathcal{V}}. \quad (6)$$

As depicted in Fig. 1, we wish to develop a theory that holds over some arbitrarily larger spatial region Ω (with volume $V > \mathcal{V}$) and time interval Λ (with duration $\lambda \geq \tau_m$). While the ergodic hypothesis must hold at the scale of \mathcal{V} , the system may be nonergodic when considered at the larger scale of Ω . Due to the potential failure of the ergodic hypothesis, statistical mechanics is less well suited to derive relevant hydrodynamic theory at larger scales. In this situation, it is desirable to define averages such that the ergodic hypothesis applies at a small scale but not at larger scales. To define

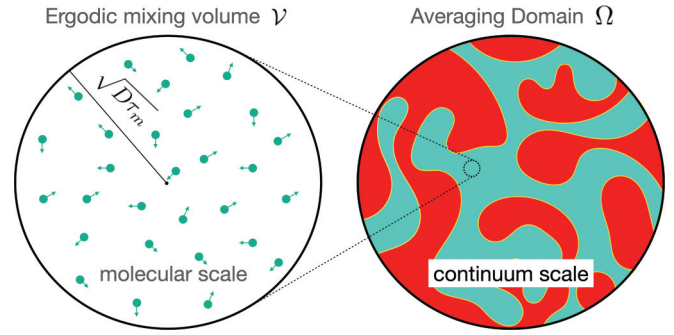


FIG. 1. The length scale for ergodicity can be estimated based on $\sqrt{D\tau_m}$, the mean distance for diffusion over timescale τ_m . We consider heterogeneous systems where the ergodic hypothesis holds at the scale of \mathcal{V} , but not at the larger scale of Ω .

larger-scale measures, we apply the time-and-space averaging operator,

$$\langle f \rangle \equiv \frac{1}{\lambda \mathcal{V}} \int_{\Lambda} \int_{\Omega} f dV dt. \quad (7)$$

We note that this convention does not define an ensemble average, but instead represents an explicit average over a region in time and space. The integral is therefore constructed to include the actual dynamics of the system, such that insights into the system behavior can be inferred based on conservation of energy with minimal assumptions. Averages are defined such that extensive quantities retain the same physical meaning across scales,

$$\bar{U} \equiv \langle U \rangle, \quad \bar{S} \equiv \langle S \rangle, \quad \bar{X}_i \equiv \langle X_i \rangle. \quad (8)$$

The intensive quantities are then defined as a weighted average with the conjugated extensive quantity from Eq. (8),

$$\bar{T} \equiv \frac{\langle TS \rangle}{\langle S \rangle}, \quad \bar{Y}_i \equiv \frac{\langle X_i Y_i \rangle}{\langle X_i \rangle}. \quad (9)$$

These definitions ensure that the representation of the system energy is scale consistent, e.g., the product of entropy and temperature corresponds to the thermal energy [41]. Since entropy is additive, the temperature should be defined as the average thermal energy per unit of entropy. The averaged form is thus consistent with Eq. (3),

$$\bar{U} = \bar{T} \bar{S} + \bar{X}_i \bar{Y}_i. \quad (10)$$

Nonequilibrium behavior can be considered by averaging the differential form of Eq. (3),

$$\begin{aligned} \frac{\partial \bar{U}}{\partial t} &= \left\langle T \frac{\partial S}{\partial t} \right\rangle + \left\langle Y_i \frac{\partial X_i}{\partial t} \right\rangle \\ &= \bar{T} \frac{\partial \bar{S}}{\partial t} + \left\langle (T - \bar{T}) \frac{\partial S}{\partial t} \right\rangle \\ &\quad + \bar{Y}_i \frac{\partial \bar{X}_i}{\partial t} + \left\langle (Y_i - \bar{Y}_i) \frac{\partial X_i}{\partial t} \right\rangle. \end{aligned} \quad (11)$$

We now define multiscale deviation terms as

$$T' \equiv T - \bar{T}, \quad Y'_i \equiv Y_i - \bar{Y}_i. \quad (12)$$

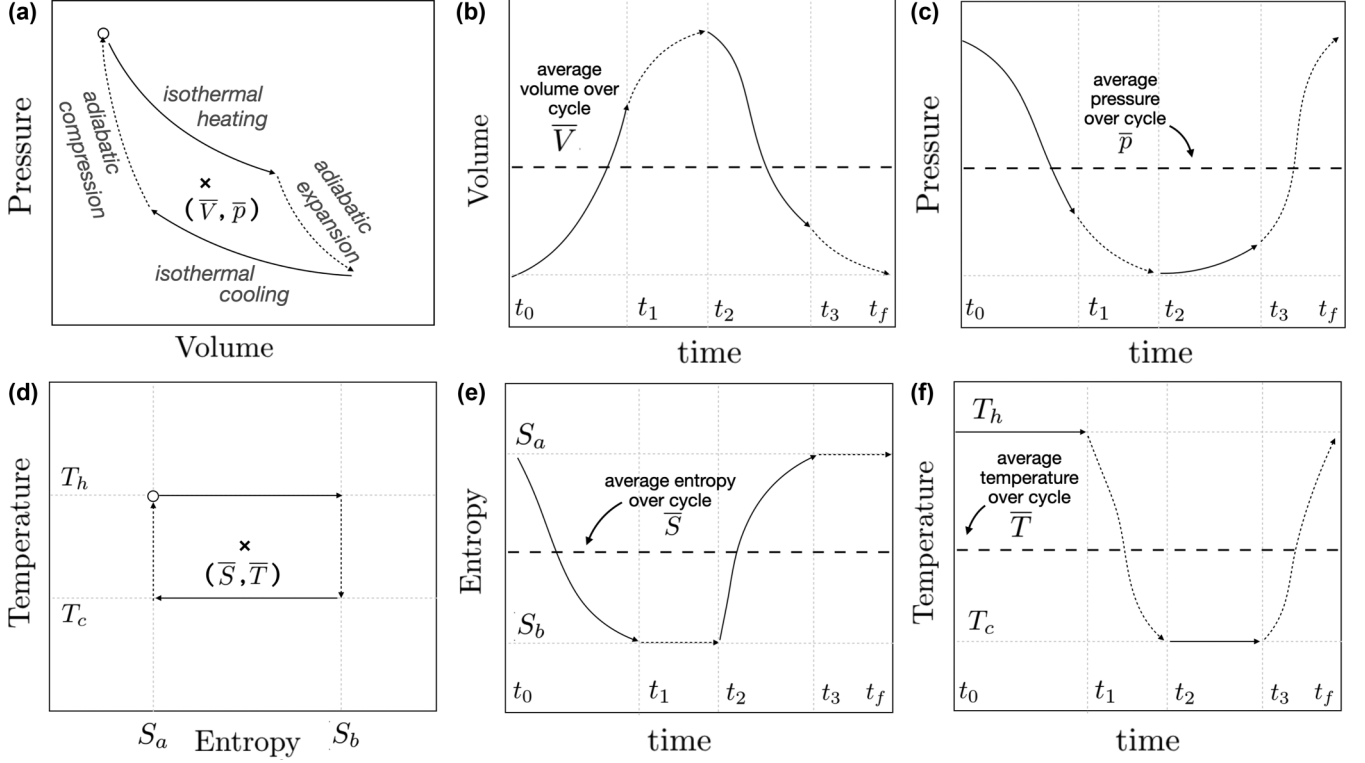


FIG. 2. Carnot cycle as a fluctuation: time averaging around the entire cycle results in constant average values of the entropy \bar{S} and temperature \bar{T} ; volume \bar{V} and pressure \bar{p} . For any cyclic process, a stationary time series will be obtained for all thermodynamic quantities. Using a time average, the energy dynamics can be embedded within fluctuation terms that capture the net energy contribution over the cycle.

Using the definitions from Eqs. (8) and (9), we can show that

$$\left\langle T' \frac{\partial S}{\partial t} \right\rangle = - \left\langle S \frac{\partial T'}{\partial t} \right\rangle, \quad \left\langle Y'_i \frac{\partial X_i}{\partial t} \right\rangle = - \left\langle X_i \frac{\partial Y'_i}{\partial t} \right\rangle, \quad (13)$$

which can be substituted into Eq. (11) and rearranged to obtain an entropy inequality,

$$\frac{\partial \bar{S}}{\partial t} = \frac{1}{\bar{T}} \left[\frac{\partial \bar{U}}{\partial t} - \bar{Y}_i \frac{\partial \bar{X}_i}{\partial t} + \underbrace{\left\langle S \frac{\partial T'}{\partial t} \right\rangle + \left\langle X_i \frac{\partial Y'_i}{\partial t} \right\rangle}_{\text{fluctuation terms}} \right] \geq 0. \quad (14)$$

The result is easily recognizable as the fundamental relation of nonequilibrium thermodynamics (e.g., [42]), but with additional terms associated with fluctuations. The fluctuations contribute to the energy dynamics whenever intensive variables deviate nonlinearly from their average values within the spatial region Ω and time interval Λ .

III. THE CARNOT CYCLE AS A FLUCTUATION

Spatial averages have been explored extensively in the context of classical nonequilibrium thermodynamics [41]. Extending this approach to also include time averages provides a way to smooth the temporal dynamics of the system. To illustrate how this works, we consider the familiar example of the Carnot cycle, as depicted in Fig. 2. The cycle begins at time t_0 and completes at time t_f , repeating in periodic fashion. The time average does not depend on the region of time Λ as long as the duration λ is an integer multiple of the period $t_f - t_0$. We choose $\lambda = t_f - t_0$ so that $1/\lambda$ corresponds to the cycle frequency. For the Carnot cycle, the thermodynamic

state is described by $U(S, V)$. The nonequilibrium behavior is described in an average form according to Eq. (14),

$$\frac{\partial \bar{U}}{\partial t} - \bar{T} \frac{\partial \bar{S}}{\partial t} + \bar{p} \frac{\partial \bar{V}}{\partial t} + \left\langle S \frac{\partial T'}{\partial t} \right\rangle - \left\langle V \frac{\partial p'}{\partial t} \right\rangle = 0, \quad (15)$$

where \bar{U} , \bar{S} , \bar{V} , \bar{T} , and \bar{p} are time-and-space average values for the complete cycle. Since the associated time series is stationary, these are each constant when the time averaging interval is an integer multiple of $\lambda = t_f - t_0$. This means that

$$\frac{\partial \bar{U}}{\partial t} = 0, \quad \frac{\partial \bar{S}}{\partial t} = 0, \quad \frac{\partial \bar{V}}{\partial t} = 0. \quad (16)$$

In other words, \bar{S} , \bar{V} , \bar{T} , and \bar{p} are the average values around which the system is fluctuating, as shown in Figs. 2(a)–2(f). The energy dynamics are fully described by the relationship between the fluctuations,

$$\left\langle V \frac{\partial p'}{\partial t} \right\rangle = \left\langle S \frac{\partial T'}{\partial t} \right\rangle. \quad (17)$$

We now separately consider each fluctuation. First, the pressure fluctuation is identical to the rate of pressure volume work W (with the sign convention chosen to obtain positive external work),

$$\left\langle V \frac{\partial p'}{\partial t} \right\rangle = - \left\langle p \frac{\partial V}{\partial t} \right\rangle = \left\langle \frac{\partial W}{\partial t} \right\rangle. \quad (18)$$

This is a consequence of the fact that the averages \bar{p} and \bar{V} are each constant. The pressure fluctuation therefore directly corresponds to the power output. Next, we treat the temperature fluctuation. For the Carnot cycle, all temperature

changes occur during isentropic conditions. Using the additive property for the time integral, it is straightforward to show that

$$\begin{aligned} \left\langle S \frac{\partial T'}{\partial t} \right\rangle &= \left\langle S \frac{\partial T}{\partial t} \right\rangle \\ &= \frac{1}{\lambda} \left(\int_{t_1}^{t_2} S_a \frac{\partial T}{\partial t} dt + \int_{t_3}^{t_f} S_b \frac{\partial T}{\partial t} dt \right) \\ &= \frac{1}{\lambda} (S_b - S_a)(T_h - T_c). \end{aligned} \quad (19)$$

Inserting these into Eq. (15) and using the fact that the heat added to the system is given by $Q_h = T_h(S_b - S_a)$, we obtain

$$\left\langle \frac{\partial W}{\partial t} \right\rangle = \frac{1}{\lambda} \frac{Q_h(T_h - T_c)}{T_h}. \quad (20)$$

This is identical to the standard result for the efficiency of a Carnot engine, but is formulated as an expression for the power output based on the cycle frequency λ . This demonstrates that in a time averaged formulation, any energy dynamics that occur faster than the duration for the time averaging window will be recast as fluctuations. Since the integral defined by Eq. (7) explicitly accounts for the path of the system, the energy dynamics are fully captured by the homogenized representation. With respect to the second law of thermodynamics, a critical insight from this exercise is that the interpretation of the entropy is scale dependent since the rate of entropy production depends explicitly on the timescale at which a process is considered. This will be particularly important in heterogeneous systems where there are crossover times due to the scaling behavior for dominant physical processes. For any stationary process, the rate of entropy production will be zero if the dynamics are considered over a sufficiently long timescale. We note that this does not contradict the Clausius theorem since the relationship between the rate of heat added and the rate of work is unchanged based on the time average. In other words, a scale-consistent representation of the energy dynamics is recovered.

IV. FLUCTUATIONS OF MAXWELL'S DEMON

To further illustrate the role of fluctuations, we consider the actions of Maxwell's demon based on the two-chamber system shown in Fig. 3 [43,44]. The demon operates a gate, selectively allowing fast-moving molecules to move from the cold chamber to the hot chamber. In apparent violation of thermodynamic intuition, the associated transfer of kinetic energy increases the temperature of the hot chamber. Maxwell's demon can be considered in the context of nonergodic behavior, as the demon controls the mixing of information between the two chambers. The demon defines locally nonstationary behavior by applying molecular scale rules that prevent a forward process from reaching equilibrium with the corresponding reverse process. However, this does not mean the process is irreversible; it only means that the equilibrium has been delayed. We will show that if a conservative demon is disabled, the system will return to its original state. Fluctuations are an appropriate tool for understanding the energy dynamics in such a system. Furthermore, the system is spatially heterogeneous and the chambers can be denoted as subregions of the system, Ω_h and Ω_c . Based on these

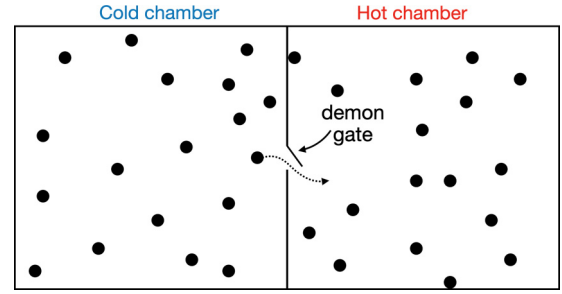


FIG. 3. “Maxwell’s demon” considers a thought experiment in which a demon selectively permits the migration of hot molecules from one chamber to the other. Due to the heat flux carried by the transmitted molecules, the temperature of the hot chamber increases, leading to a thermal gradient between the chambers. The demon’s actions are constrained by a symmetry law relating thermal fluctuations.

definitions, a discrete aspect is introduced into the system representation since the crossing of molecules from one subregion to the other occurs as discrete events. Time averaging smooths the effect of these crossings such that the action of the demon can be modeled as being continuous with respect to time.

For an ideal monatomic gas, the entropy is given by the Sackur-Tetrode equation [45–47],

$$S(U, V, N) = k_B N \left[\frac{5}{2} + \ln \frac{V}{N} + \frac{3}{2} \ln \frac{U}{N} + \frac{3}{2} \ln \frac{2\pi m}{h^2} \right], \quad (21)$$

where m is the particle mass and h is Planck’s constant. The expression for entropy as a state function is sufficient to determine the form $U(S, V, N)$. The intensive quantities can be determined directly from their thermodynamic definitions,

$$\begin{aligned} T &\equiv \left(\frac{\partial U}{\partial S} \right)_{N,V} = \frac{2U}{3k_B N}, \\ p &\equiv - \left(\frac{\partial U}{\partial V} \right)_{N,S} = \frac{k_B N T}{V}, \\ \mu &\equiv \left(\frac{\partial U}{\partial N} \right)_{S,V} = -k_B T \left(\ln \frac{V}{N} + \frac{3}{2} \ln \frac{U}{N} + \frac{3}{2} \ln \frac{2\pi m}{h^2} \right). \end{aligned} \quad (22)$$

Noting that $U = \frac{3}{2} k_B N T$ for an ideal gas, it is easy to show that these forms are consistent with Eq. (2) in the particular form $U = TS - pV + \mu N$. To treat the demon, we must subdivide the system based on thermodynamics within each chamber. This is accomplished by subsetting the system into regions based on the indicator function Υ_i ,

$$\Upsilon_i(\mathbf{x}) = \begin{cases} 1 & \text{if } \mathbf{x} \in \Omega_i \\ 0 & \text{otherwise,} \end{cases} \quad (23)$$

for $i \in \{h, c\}$. Consistent with Eqs. (8) and (9), separate temperature, entropy, pressure, chemical potential, and number of molecules are obtained for each chamber. For extensive properties, fields are constructed based on the subset operation,

$$\frac{S_i}{\mathcal{V}} \equiv \frac{S \Upsilon_i}{\mathcal{V}}, \quad \frac{N_i}{\mathcal{V}} \equiv \frac{N \Upsilon_i}{\mathcal{V}}, \quad V_i = \mathcal{V} \Upsilon_i, \quad (24)$$

where \mathcal{V} has been included explicitly in the definitions to account for the fact that the reference volume used to define fields should not be infinitely small (i.e., should exceed the molecular length scale). Averages are then defined as time- and-space averages,

$$\begin{aligned}\bar{S}_i &\equiv \langle S_i \rangle, & \bar{T}_i &\equiv \frac{\langle TS_i \rangle}{\langle S_i \rangle}, \\ \bar{V}_i &\equiv \langle V_i \rangle, & \bar{p}_i &\equiv \frac{\langle pV_i \rangle}{\langle V_i \rangle}, \\ \bar{N}_i &\equiv \langle N_i \rangle, & \bar{\mu}_i &\equiv \frac{\langle \mu N_i \rangle}{\langle N_i \rangle}.\end{aligned}\quad (25)$$

For simplicity, we consider the case where the volume for each chamber is constant, with $V_c = V_h$. These definitions ensure that the entropy is additive,

$$\bar{S} = \bar{S}_c + \bar{S}_h, \quad (26)$$

and that the total thermal energy is conserved based on the definition of the temperature,

$$\bar{T}\bar{S} = \bar{T}_c\bar{S}_c + \bar{T}_h\bar{S}_h. \quad (27)$$

For the number of molecules and chemical potential,

$$\bar{\mu}\bar{N} = \bar{\mu}_c\bar{N}_c + \bar{\mu}_h\bar{N}_h. \quad (28)$$

It is clear that generic thermodynamic quantities can be defined by subsetting a heterogeneous system into regions. The result of the subsetting operation is functionally equivalent to an alternative specification of the extensive variables,

$$U = U(S_h, S_c, V_h, V_c, N_h, N_c). \quad (29)$$

However, since the set operation defined from Υ_i introduces a discrete element into the system representation, apparent discontinuities can result when considering energy exchanges between the entities. Averaging in time removes these discontinuities to ensure a smooth representation for the dynamics within subregions. As an example, even though the Hamiltonian for the molecular system is continuous, the molecular crossing shown in Fig. 3 is a discrete event. Combining the subset operation with a time average leads to a corresponding fluctuation theorem because any energy gained by the hot chamber is directly lost by the cold chamber. The fluctuation terms impose a symmetry constraint on the demon's action on the basis that the demon must conserve mass and energy.

Since the system is closed, the total number of particles is conserved,

$$\frac{\partial \bar{N}_h}{\partial t} = -\frac{\partial \bar{N}_c}{\partial t}. \quad (30)$$

Subdivision of the system into hot and cold compartments leads to the following fluctuation constraint based on conservation of energy:

$$\begin{aligned}\frac{\partial \bar{S}}{\partial t} &= \frac{1}{T} \sum_i \left[\left\langle S_i \frac{\partial T'_i}{\partial t} \right\rangle - \left\langle V_i \frac{\partial p'_i}{\partial t} \right\rangle + \left\langle N_i \frac{\partial \mu'_i}{\partial t} \right\rangle \right] \\ &+ \left(\frac{\bar{\mu}_h - \bar{\mu}_c}{T} \right) \frac{\partial \bar{N}_c}{\partial t},\end{aligned}\quad (31)$$

where $T'_i = T_i - \bar{T}$, $\mu'_i = \mu_i - \bar{\mu}$, and $p'_i = p_i - \bar{p}$ on Ω_i with $i \in \{c, h\}$.

It has been argued from an information theory perspective that the demon must be able to perform measurements in order to function as described by Maxwell [48]. For example, the demon would need to know the temperature of the hot chamber so that it could determine which molecules should pass through the gate. However, a simple thought experiment demonstrates that a demon can generate gradients without relying on any nonlocal information or altering the energy for any molecules that it comes into contact with. Consider a demon that is tuned to operate at some particular temperature T_d . The demon will allow any molecule with speed greater than one standard deviation above the mean for the Maxwell distribution of speeds to pass from the cold chamber to the hot chamber, i.e., molecules with speed,

$$v_d \geq \sqrt{\frac{3k_B T_d}{m}}. \quad (32)$$

The statistics for the crossings can be determined from the Maxwell distribution. If the demon operates at temperatures in the vicinity of T_d , it can drive the formation of a gradient without any knowledge of the system state. The demon only needs to measure the molecular speed, which may be done locally and reversibly without retaining any memory of the measurement. Of course, this action cannot be performed without a constraint: molecules with sufficient speed must hit the portion of the wall where the demon gate is located since the demon cannot impose any forces to attract particles toward its location. The probability for fast molecules to hit the demon gate depends on T_c based on the Maxwell distribution of speeds and also on the area of the gate relative to the area of the partition between the two chambers. As T_c decreases, so too will the rate at which sufficiently energetic molecules hit the gate. With the demon's behavior defined statistically based on Eq. (32), we can calculate the rate for mass exchange. The number of particles moving from the cold chamber to the hot chamber is

$$\begin{aligned}\frac{\partial N_{ch}}{\partial t} &= \frac{N_c A_g}{V_c} \int_{v_d}^{\infty} \sqrt{\frac{m}{2\pi k_B T_c}} s e^{-ms^2/2k_B T_c} ds \\ &= -\frac{N_c A_g}{V_c} \sqrt{\frac{k_B T_c}{2\pi m}} e^{-mv_d^2/2k_B T_c},\end{aligned}\quad (33)$$

where A_g is the area of the gate between the chambers. Similarly, the rate of energy exchange is

$$\begin{aligned}\frac{\partial U_{ch}}{\partial t} &= \frac{N_c A_g}{V_c} \int_{v_d}^{\infty} \sqrt{\frac{m}{2\pi k_B T_c}} \frac{ms^3}{2} e^{-ms^2/2k_B T_c} ds \\ &= -\frac{m N_c A_g}{V_c \sqrt{2\pi}} \left(\frac{k_B T_c}{m} \right)^{3/2} \left(1 + \frac{mv_d^2}{2k_B T_c} \right) e^{-mv_d^2/2k_B T_c}.\end{aligned}\quad (34)$$

We consider a two-way valve so that a steady state can be achieved based on the redistribution of slower molecules to the cold chamber. A simple way to achieve this is to allow any molecule that hits the gate to travel back to the cold chamber. This clearly requires no measurement and meets

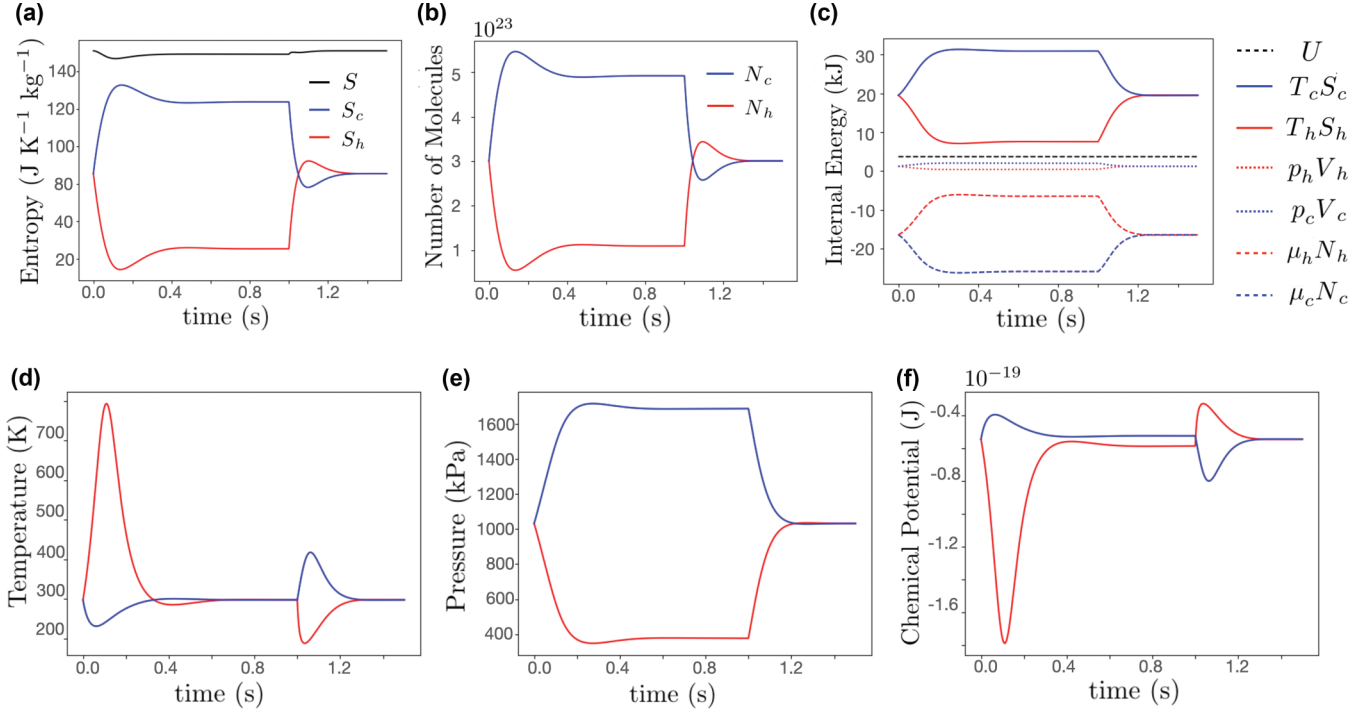


FIG. 4. Fluctuations due to operation of a conservative Maxwell's demon: the demon is activated at $t = 0$ second and deactivated at time $t = 1.0$ second to obtain a stationary time series. Fluctuations to the intensive properties are observed based on the redistribution of mass and energy within the system.

the constraints used previously. The statistics for the particles gained by the cold chamber are given by

$$\frac{\partial N_{hc}}{\partial t} = \frac{N_h A_g}{V_h} \sqrt{\frac{k_B T_h}{2\pi m}}, \quad (35)$$

$$\frac{\partial U_{hc}}{\partial t} = \frac{m N_h A_g}{\sqrt{2\pi} V_h} \left(\frac{k_B T_h}{m} \right)^{3/2}. \quad (36)$$

Since the rules used to define this behavior do not require nonlocal information, the demon will be able to spatially segregate particles based on conservation of energy and without violating physical laws. Fast particles will accumulate in the hot chamber and slow particles will accumulate in the cold chamber. The primary mechanism needed to achieve this is to prevent slow molecules from entering the hot chamber. The role played by the demon is therefore to delay equilibrium by preventing energy from partitioning itself equally between the two chambers. Compared to the initial state, the forward process (particles move from hot to cold) cannot reach an equilibrium with the reverse process (particles move from cold to hot). This produces a nonstationary process. However, since no energy is removed or added, stationary behavior can be restored by simply disabling the demon.

We now treat the fluctuations that are created due to operation of the hypothetical demon. Based on Eqs. (33) and (36), the total mass and energy exchange between chambers is defined for each time step δt ,

$$\delta N_c = \left[\frac{N_h A_g}{V_h} \sqrt{\frac{k_B T_h}{2\pi m}} - \frac{N_c A_g}{V_c} \sqrt{\frac{k_B T_c}{2\pi m}} e^{-mv_d^2/2k_B T_c} \right] \delta t,$$

$$\delta U_c = \frac{m A_g}{\sqrt{2\pi} V_h} \left[N_h \left(\frac{k_B T_h}{m} \right)^{3/2} - N_c \left(\frac{k_B T_c}{m} \right)^{3/2} \left(1 + \frac{mv_d^2}{2k_B T_c} \right) e^{-mv_d^2/2k_B T_c} \right] \delta t. \quad (37)$$

The energy and particle number are updated so that conservation is strictly obeyed,

$$\begin{aligned} N_c(t + \delta t) &\leftarrow N_c(t) + \delta N_c, \\ N_h(t + \delta t) &\leftarrow N_h(t) - \delta N_c, \\ U_c(t + \delta t) &\leftarrow U_c(t) + \delta U_c, \\ U_h(t + \delta t) &\leftarrow U_h(t) - \delta U_c. \end{aligned} \quad (38)$$

The system is closed by assuming that Eqs. (21) and (22) hold separately within each subregion. The initial condition sets equilibrium conditions in each chamber with 1 mol of helium atoms equally divided between the two chambers at $T_d = 298$ K. The demon is activated at $t = 0$ with $\delta t = 0.00025$ sec. The demon operates until $t = 1.0$ second, ultimately reaching a steady state. The difference in pressures is accounted for by the differential momentum transfer that results from the demons operation according to Eqs. (33)–(38). Once the steady state is achieved, the demon is disabled and the system returns exactly to its initial state and producing a stationary time series (see the Supplemental Material for the complete implementation [49]). For the results shown in Fig. 4, the system is explicitly ergodic by construction since the Maxwell distribution has been assumed (meaning equipartition of energy is strictly observed within each chamber). At this fast timescale, entropy production occurs based on the

redistribution of mass and energy between the two chambers [see Fig. 4(a)]. We note that molecular rules do not necessarily need to satisfy positive entropy production since entropy is a statistical concept that does not apply at the deterministic scale of an individual molecule. However, since no heat is added to the two-chamber system, the Clausius theorem remains valid. Unlike the Carnot engine, the demon does not require added heat or work to generate the fluctuation. The demon is simply delaying the equilibrium of the system. Since no energy has been removed from the system, it can be treated as a reversible process when considered over longer time intervals.

If the timescale for averaging is small, fluctuations to intensive properties will be zero based on the fact that the rate of change is locally linear over short timescales. Fluctuation terms contribute when considering behavior over long timescales. At the end of the cycle, the entropy and particle number return exactly to their original value, meaning that

$$\frac{\partial \bar{S}}{\partial t} = 0, \quad \frac{\partial \bar{N}_c}{\partial t} = 0. \quad (39)$$

In other words, zero entropy production is observed when the system is considered over the longer timescale. Inserting Eq. (39) into Eq. (31) leads to fluctuation criterion at long times,

$$\left\langle S_i \frac{\partial T'_i}{\partial t} \right\rangle - \left\langle V_i \frac{\partial p'_i}{\partial t} \right\rangle + \left\langle N_i \frac{\partial \mu'_i}{\partial t} \right\rangle = 0. \quad (40)$$

This result simply means that thermal fluctuations must obey conservation of energy, consistent with the results established from the perspective of microscopic reversibility [50,51]. The result is a simple fluctuation theorem that is distinct from approaches proposed by other treatments [52–57]. A basic challenge presented by Eq. (40) is that the fluctuation criterion depends on the total entropy since this is needed to compute $\langle S_i \frac{\partial T'_i}{\partial t} \rangle$. While the Sackur-Tetrode equation provides an adequate approximation for an ideal gas, the situation for thermal fluctuations is not easily generalized. The demon illustrates two important features of systems where multiscale fluctuations are important. First, it defines an energy barrier that prevents mixing between the hot and cold chambers. Second, the problem is associated with gradients in an intensive thermodynamic property. We now demonstrate the importance of these terms in capillary-dominated systems, where gradients in composition and chemical potential lead to length scale heterogeneity.

V. MASS DIFFUSION

The advantages of time-and-space averaging are particularly intriguing for spatially heterogeneous systems. In this section, we consider the application to mass diffusion, which is a common source of spatial heterogeneity. Compositional gradients are a key feature in these systems and these heterogeneities cause fluctuations when the system is stimulated. In such cases, the fluctuation terms can be directly linked to classical microscopic nonequilibrium thermodynamics using phenomenological equations established based on the theory of Onsager [58]. Phenomenological equations provide the basis to establish the rates at which particular processes occur, linking the temporal, spatial, and energy scales. Fick's law

can be directly recovered at length scales that are accessible based on molecular dynamics simulations [59]. In the context of Onsager, phenomenological equations are derived based on a local near-equilibrium assumption. The associated reciprocal relations can be derived based on an assumption of microscopic reversibility. These conditions are presumed to hold at the scale of \mathcal{V} since this scale is defined based on the local diffusion coefficient. The relevant linear phenomenological equation is Fick's law, which is assumed to describe the nonequilibrium behavior at the small scale of \mathcal{V} ,

$$\frac{\partial \rho_k}{\partial t} - \nabla \cdot (\mathbf{D}_k \cdot \nabla \mu_k) = 0, \quad (41)$$

where \mathbf{D}_k is the mass diffusion tensor, ρ_k is the density, and μ_k is chemical potential. Fick's law asserts that there is a locally linear nonequilibrium response to compositional gradients. However, we note that in a heterogeneous system, linear response theory will fail at larger scales due to nonlinearity in the composition, diffusion coefficient, and chemical potential. Such nonlinearities will inevitably lead to anomalous diffusion phenomena, and associated nonequilibrium behaviors can be understood in terms of multiscale fluctuations.

The standard nonequilibrium treatment for mass diffusion is obtained by considering the internal energy to be described by $U(S, N_k)$, with N_k being the number of molecules of component k . For a closed system, Eq. (14) can be written as

$$\frac{\partial \bar{S}}{\partial t} = \frac{1}{T} \left[\left\langle S \frac{\partial T'}{\partial t} \right\rangle - \bar{\mu}_k \frac{\partial \bar{N}_k}{\partial t} + \left\langle N_k \frac{\partial \mu'_k}{\partial t} \right\rangle \right] \geq 0. \quad (42)$$

In an isothermal system, the temperature fluctuation is zero. The remaining terms can be directly interpreted based on Fick's law,

$$\begin{aligned} \bar{\mu}_k \frac{\partial \bar{N}_k}{\partial t} - \left\langle N_k \frac{\partial \mu'_k}{\partial t} \right\rangle &= \bar{\mu}_k \frac{\partial \bar{N}_k}{\partial t} - \left\langle N_k \frac{\partial (\mu_k - \bar{\mu}_k)}{\partial t} \right\rangle \\ &= \bar{\mu}_k \frac{\partial \bar{N}_k}{\partial t} + \bar{N}_k \frac{\partial \bar{\mu}_k}{\partial t} - \left\langle N_k \frac{\partial \mu_k}{\partial t} \right\rangle \\ &= \frac{\partial (\bar{\mu}_k \bar{N}_k)}{\partial t} - \frac{\partial \langle \mu_k N_k \rangle}{\partial t} + \left\langle \mu_k \frac{\partial N_k}{\partial t} \right\rangle. \end{aligned}$$

The first two terms cancel based on the fact that $\bar{\mu}_k \bar{N}_k = \langle \mu_k N_k \rangle$ according to the definition given in Eq. (9). Now assuming that Fick's law holds at the microscopic scale with $\rho_k = N_k/\mathcal{V}$, we arrive at

$$\frac{1}{\mathcal{V}} \left\langle \mu_k \frac{\partial N_k}{\partial t} \right\rangle = \left\langle \mu_k \nabla \cdot (\mathbf{D}_k \cdot \nabla \mu_k) \right\rangle. \quad (43)$$

By inserting this into Eq. (42), it is evident that the dissipation is entirely determined from the contribution of the spatial gradients. In other words, the length scale associated with gradients is fundamentally linked with the timescale for energy dissipation based on the phenomenological coefficient. Furthermore, assuming Fick's law at the microscopic scale does not imply it will hold at larger scales. To see this, we can formally average the right-hand side of Eq. (43),

$$\begin{aligned} \langle \mu_k \nabla \cdot (\mathbf{D}_k \cdot \nabla \mu_k) \rangle &= \bar{\mu}_k \nabla \cdot (\bar{\mathbf{D}}_k \cdot \nabla \bar{\mu}_k) + \bar{\mu}_k \nabla \cdot (\bar{\mathbf{D}}_k \cdot \nabla \langle \mu'_k \rangle) \\ &\quad + \bar{\mu}_k \langle \nabla \cdot (\mathbf{D}'_k \cdot \nabla \mu_k) \rangle \\ &\quad + \langle \mu'_k \nabla \cdot (\mathbf{D}_k \cdot \nabla \mu_k) \rangle. \end{aligned}$$

Scale invariance for Fick's law will therefore be obtained if the following conditions are satisfied:

$$\langle \nabla \mu'_k \rangle = 0, \quad (44)$$

$$\langle \nabla \cdot (\mathbf{D}'_k \cdot \nabla \mu_k) \rangle = 0, \quad (45)$$

$$\langle \mu'_k \nabla \cdot (\mathbf{D}_k \cdot \nabla \mu_k) \rangle = 0, \quad (46)$$

where the deviation for the diffusion tensor is $\mathbf{D}'_k = \mathbf{D}_k - \bar{\mathbf{D}}_k$. In ideal systems, the chemical potential is directly related to the density,

$$\mu = \mu_0 + RT \ln(\rho/\rho_0), \quad (47)$$

with μ_0 and ρ_0 being constant reference values. Ideal conditions imply that Eq. (44) must hold due to the definition of $\bar{\rho}_k$. Equation (45) will hold if \mathbf{D}_k is independent of space and time since this would mean that $\mathbf{D}'_k = 0$. Finally, Eq. (46) suggests that the existence of gradients in \mathbf{D}_k or μ_k that have a length scale smaller than Ω will cause Fick's law to fail at the averaged scale, as will transient changes to these gradients that occur faster than the averaging timescale Λ . At the intuitive level, these criteria require that the diffusion coefficient, composition, and chemical potential should vary only linearly over Λ and Ω . For such cases, the fluctuation terms disappear and Fick's law will hold in the larger-scale system. However, in real systems, non-Fickian behavior is quite common [60–62]. Diffusive and dispersive processes within a complex microstructure give rise to the development of heterogeneous structures, including fractals, based on local instabilities and material heterogeneity [63]. The implication is that Eqs. (44) and (45) do not hold under typical conditions since mass transport routinely leads to transient spatial heterogeneity for the composition, chemical potential, and diffusion coefficient.

VI. CAPILLARY FLUCTUATIONS

In heterogeneous systems, it is common for chemical potential gradients to exist at multiple length scales. Multiphase systems arise due to the dependence of μ on composition, e.g., in the Cahn-Hilliard equations,

$$\mu = \phi^3 - \phi - \gamma \nabla^2 \phi. \quad (48)$$

The order parameter $\phi = \rho - (\rho_l^* + \rho_g^*)/2$, where the equilibrium densities for the liquid and gas are ρ_l^* and ρ_g^* . The parameter γ determines the width of the interface separating the two pure phase regions. It is entirely possible to describe multiphase systems using Eq. (48) in combination with Eq. (42). As a matter of convenience, we can also describe the thermodynamics of the system by considering Eq. (2) in the form

$$U = U(S, V_w, V_n, A_{wn}), \quad (49)$$

where V_w and V_n are the volume of the droplet and the surrounding fluid and A_{wn} is the interfacial area between the fluids. The associated intensive variables are the pressures p_w and p_n and the interfacial tension γ_{wn} . Averaging in time and space, we assume (1) isothermal conditions, (2) constant interfacial tension, (3) the volume of each fluid is constant,

and (4) compositional effects are negligible. Subject to these restrictions, Eq. (14) simplifies to

$$\frac{\partial \bar{S}}{\partial t} = -\frac{1}{\bar{T}} \left[\left\langle V_w \frac{\partial p'_w}{\partial t} \right\rangle + \left\langle V_n \frac{\partial p'_n}{\partial t} \right\rangle + \bar{\gamma}_{wn} \frac{\partial \bar{A}_{wn}}{\partial t} \right] \geq 0. \quad (50)$$

Dissipative effects are understood by considering the fluctuation of the fluid pressures that are induced by the spontaneous change in surface energy.

The coalescence of two fluid droplets represents one of the simplest examples of topological change in fluid mechanics. The topological event induces an apparent singularity followed by a cascade of energy dissipation governed by distinct scaling regimes as the system establishes a new equilibrium. At equilibrium, the fluid pressures and interface curvature are related based on the Young-Laplace equation,

$$p_n - p_w = \gamma_{wn} \left(\frac{1}{R_1} + \frac{1}{R_2} \right), \quad (51)$$

where R_1 and R_2 are the principal curvatures along the interface between fluids. Detailed studies of the droplet coalescence mechanism show that the flow behavior and associated geometric evolution are coupled on a very fast timescale [64–71]. At the molecular level, coalescence is initiated based on thermal effects [72]. Hydrodynamic effects become dominant after approximately 30 picoseconds, based on the formation of a bridge that joins the droplets. The ensuing dynamics can be separated into two distinct regimes [70]. At early times, viscous effects dominate and the growth of the bridge radius scales as

$$\frac{r}{r_c} \sim \frac{t}{\tau_c}, \quad (52)$$

where τ_c is the crossover time and r_c is the associated length scale. At late times, inertial effects dominate and the growth of the bridge radius scales as

$$\frac{r}{r_c} \sim \sqrt{\frac{t}{\tau_c}}. \quad (53)$$

Analogous results have been obtained for droplet snap-off [36]. The rate of entropy production will be a nonlinear function of time based on the crossover between the two regimes. The nonequilibrium response is therefore nonlinear. Averaging in time and space can be applied to homogenize these nonlinear dynamics so that they can be treated explicitly as energy fluctuations.

The sequence depicted in Fig. 5 shows the effect of the coalescence event on the fluid pressure field as simulated by a lattice Boltzmann model [73]. Results demonstrate that simulation accurately recovers the predicted scaling behavior. In Fig. 5, the pressure field $p_i^* = p_i R_f / \gamma_{wn}$ is normalized relative to the final droplet radius, $R_f = 80$ voxels. Nonequilibrium effects develop in response to the near instantaneous curvature disruption along the interface at the point where the droplets first touch. The associated pressure shock drives the ensuing dynamics. The behavior is nonergodic because capillary energy barriers inhibit the thermal mixing between the droplets prior to the event. Rapid mixing occurs after coalescence, once the energy barrier separating the two droplets has been destroyed.

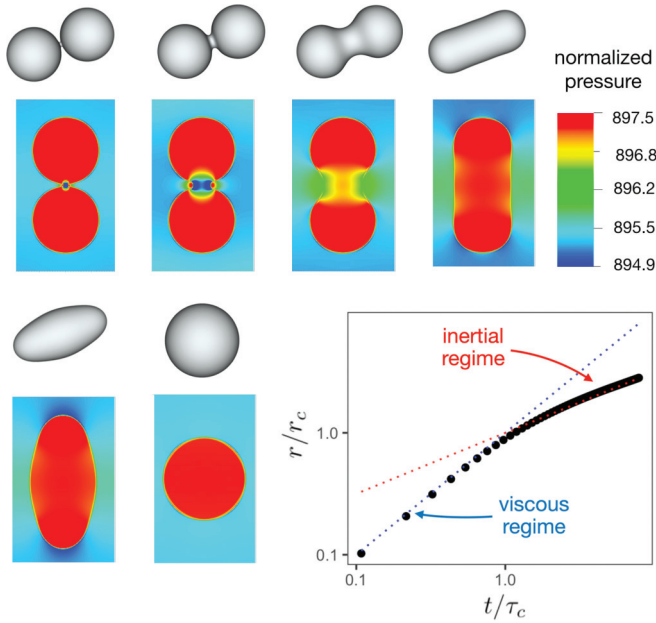


FIG. 5. Droplet coalescence leads to fluctuations in the pressure field (color) due to the rapid change in capillary forces. Scaling for the coalescence event is limited by viscous forces during the initial bridge formation, and is dominated by inertial forces at late times.

Thermal fluctuations due to molecular effects are usually assumed to be stationary with respect to time as a consequence of the time reversibility of the Hamiltonian at the molecular level [22]. Capillary fluctuations are distinct from thermal fluctuations due to the fact that they are inherently cooperative in nature, and are linked to both reversible and irreversible energy transfer. Symmetry breaking is a consequence of the structural rearrangement associated with the transition to a new local minimum energy configuration. For a closed system, the dissipated energy is easily calculated from the initial and final configurations since at equilibrium the droplets are spherical,

$$\Delta S = \frac{1}{T} (V_w \Delta p_w + V_n \Delta p_n - \gamma_{wn} \Delta A_{wn}). \quad (54)$$

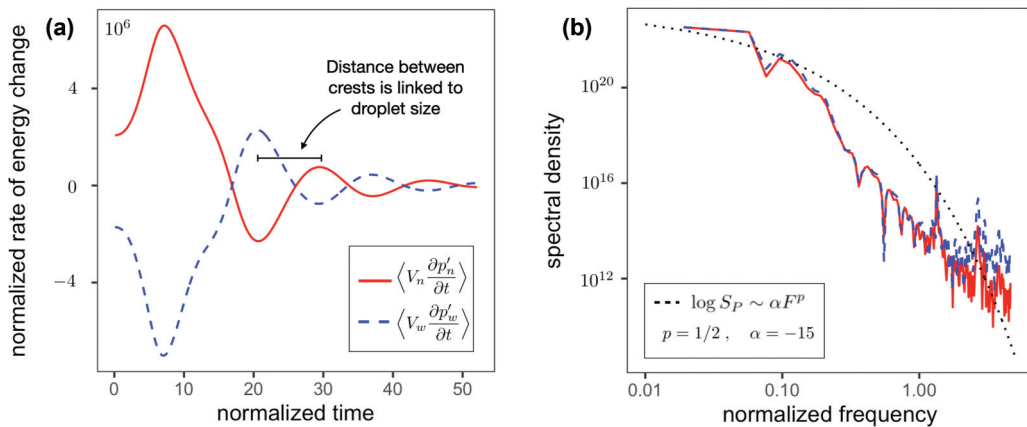


FIG. 6. Pressure fluctuation due to the coalescence of two fluid droplets. (a) Rate of energy change associated with pressure fluctuation relative to the final surface energy during droplet coalescence event. (b) Noise spectrum associated with capillary fluctuations can be predicted by $\log_{10} S_P \sim \alpha F^p$.

The radius for the initial and final droplets can be computed analytically based on the volume, making use of the Young-Laplace equation to determine the equilibrium fluid pressures.

The rate of energy change associated with capillary fluctuations is shown in Fig. 6. The timescale is normalized by the crossover time τ_c , which can be considered as defining the intrinsic timescale for coalescence. In our analysis, the full system is used as the domain for spatial averaging and the time interval is $\Lambda = 0.108\tau_c$. Since this timescale is faster than the nonlinear dynamics, the frequency for the fluctuations is directly visible in Fig. 6(a). The energy scale is normalized based on the interfacial tension and the capillary length scale, which is accomplished by dividing the energy associated with the capillary fluctuations' final surface energy $4\pi\gamma_{wn}R_f^2$. The scales in Fig. 6 are therefore nondimensional. From Eq. (50), it is clear that the changes in surface energy are driving the fluctuations. Immediately after coalescence, interfaces perform local work against the fluid pressure due to unbalanced capillary forces. The pressure fluctuation terms are understood as resulting from local gradients in the pressure field that are generated due to the curvature discontinuity. These gradients are clearly visible in Fig. 5. Since the initial and final droplet states have different capillary pressure, the pressure fluctuation is not stationary over the event. Nevertheless, a degree of symmetry is clear based on the mirroring effect between the pressure fluctuation in one fluid and the other. This suggests that the choice to represent the system in a discrete way introduces asymmetry into the system description. The Gibb's dividing surface subdivides the system into distinct subregions for each fluid, each with its own pressure. While topological changes such as droplet coalescence are fundamentally discrete events when considered from the perspective of set theory, set construction is a choice imposed on the system, as opposed to an underlying property of the physical system itself. Set operations are the basis for separately defining p_w and p_n . Detailed balance is not evident when the fluids are considered separately since irreversible energy exchanges occur between the fluids due to the cooperative rearrangement of the interface. For this reason, symmetry is a property of the global system and not a property of the subregions.

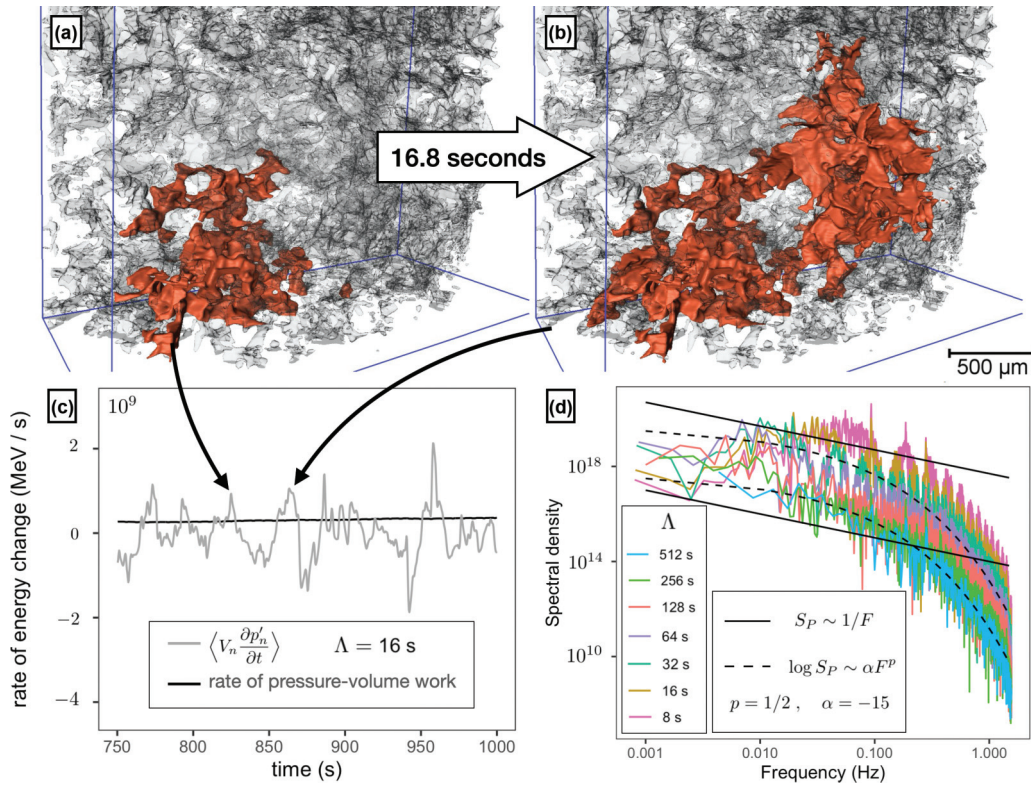


FIG. 7. Capillary fluctuations during displacement in porous media are linked with spontaneous pore-scale events that occur due to capillary forces within the solid microstructure. Haines jumps occur spontaneously during immiscible displacement as the system “jumps” from (a) one energy minimum to (b) the subsequent quasistatic configuration; (c) fluid pressure fluctuations arise due to these dynamics; and (d) scaling behavior for the power spectrum is independent of the time averaging interval.

Pressure fluctuations are multiscale rate effects that arise due to spatial heterogeneity. The length scale associated with the heterogeneity is the driving factor that determines the spectral properties. Due to length scale effects, the noise signature associated with capillary fluctuations is distinct from pink noise, where the relationship between the spectral density S_P and frequency F is $S_P \sim 1/F$ [74–76]. For the data shown in Fig. 6, the time and energy scales are nondimensionalized, as described previously. A simple power law is insufficient to describe noise due to capillary fluctuations. Instead, we find that the scaling relationship is a stretched exponential,

$$\log_{10} S_P \sim \alpha F^p. \quad (55)$$

The coefficients α and p are associated with the rate of decay in the spectral density as the frequency increases. S_P decays rapidly with F for frequencies that are faster than a typical event. This can be considered as a transition between two distinct scaling regimes. At the length and time scale for the coalescence event, the behavior is superdiffusive based on the fact that cooperative capillary forces move mass faster than the local diffusion rate. Ultimately, the capillary forces that drive these events originate due to gradients in the composition at smaller scales. At smaller length scales, subdiffusive behavior is obtained based on the strong antidiffusion associated with the interface region. The crossover between these distinct scaling regimes leads to a corresponding transition in the fluctuation spectrum. For droplet coalescence, $\alpha = -15$

and $p = 1/2$ match well with the simulated fluctuation spectrum.

The scaling relationship given by Eq. (55) also holds for immiscible displacement in porous media. Cooperative events occur routinely as fluids migrate through a complex microstructure under the influence of capillary forces [26]. Experimental data demonstrate that the timescale for these events is directly linked to the frequency for fluctuations in the pressure signal [77]. The results shown in Fig. 7 were obtained using synchrotron microtomography imaging. For complete experimental details, the reader is referred to Berg *et al.* [28]. The system was initially saturated with brine, and oil was injected into the sample at a rate of $0.35 \mu\text{L}/\text{minute}$. Pressure transducer measurements were collected at an interval $\Delta t = 0.32$ sec. The absolute permeability for the Berea sandstone was $\kappa = 0.7 \mu\text{m}^2$. The initial and final states for a pore-scale event known as a Haines jump are shown in Figs. 7(a) and 7(b). Haines jumps are spontaneous events that occur when the fluid meniscus passes through narrow pore throats within the solid microstructure, where the capillary pressure is high. As fluid spontaneously flows into the adjacent pore body, the capillary pressure drops rapidly, causing a fluctuation in the signal. The timescale for pore-scale events is controlled by the solid microstructure, which means that the statistics for the associated noise signal are linked to length scale heterogeneity within the system. In spite of this considerable complexity, the scaling behavior is predicted from Eq. (55) with identical coefficients to the droplet coalescence. In the spectral analysis, a

nondimensional timescale for the experiments can be defined as

$$t^* = \frac{\gamma_{wn} t}{\mu \sqrt{\kappa}}, \quad (56)$$

where $\mu = 0.89 \text{ mN s/m}^2$ and $\gamma_{wn} = 25 \text{ mN/m}$. Since the permeability is related to the microscopic length scale, a nondimensional energy scale can be defined by normalizing based on $\gamma_{wn}\kappa$. Averaging over a longer time interval reduces the amplitude of the fluctuations, but does not change α and p . Both droplet coalescence and Haines jump events are examples of critical phenomena. The length scale for an individual Haines jump is controlled by the solid microstructure, and a single event may cause fluids to invade multiple pores very rapidly, as shown in Figs. 7(a) and 7(b). The timescale for pressure fluctuations is therefore determined based on the distribution of length scales for the solid microstructure, which is typically very heterogeneous. It should be expected that the distribution of fluids will exert a strong influence on the fluctuation spectrum, as the probability for fluid coalescence events depends on how mass is distributed within the solid microstructure. Further study is needed to understand if universal coefficients can be established in heterogeneous systems. As in droplet coalescence, the pressure fluctuations are nonstationary. For the data shown in Fig. 7, the net contribution from the fluctuations is 7.84% of the total pressure-volume work when considered over $\Lambda = 512$ seconds. In this situation, fluctuation terms must be included explicitly in the nonequilibrium thermodynamics since these terms are needed to state the conservation of energy for the system.

VII. SUMMARY AND CONCLUSIONS

We derive nonequilibrium thermodynamic expressions using time-and-space averaging, showing that fluctuations occur due to nonlinear dynamics associated with the intensive variables. Considering a particular timescale of interest, the approach is constructed to treat systems that are ergodic at small length scales but nonergodic at larger scales. Time-and-space averages are formulated by directly integrating the energy dynamics, meaning that the actual system evolution is captured within the averaged representation. The approach is scale consistent based on the fact that thermodynamic quantities retain their physical meaning, and the form of the Euler equation will be independent of the length and time scales. Fluctuations are linked with subscale gradients in systems that exhibit multiscale heterogeneity. When stimulated, these systems have a tendency to relax toward equilibrium at macroscopically slow timescales that are determined based on the length scale associated with the gradients. We illustrate how anomalous diffusion can arise in a system where Fick's law applies at some small length scale, but fails at larger scales due to spatial heterogeneity. Explicit conditions for scale invariance are obtained.

Averages in time demonstrate that the rate of entropy production is scale dependent, e.g., due to crossover times that are frequently encountered when considering the dynamic response of heterogeneous systems. For any stationary process, the time average of the rate of entropy production is zero since net changes to any thermodynamic state function imply that a system is nonstationary. Averaging does not alter the interpretation for the Clausius theorem since averages are constructed based on the conservation of energy. The treatment of stationary processes is thereby simplified since dissipation is expressed in terms of the rate of work and heat exchange, which are linked to fluctuations based on the internal energy dynamics of the system. We consider basic applications to the Carnot cycle and to Maxwell's demon to illustrate how thermodynamic cycles can be understood in the context of fluctuations.

More generally, fluctuations describe the internal energy dynamics of thermodynamic systems away from equilibrium. Since fluctuations must conserve energy, symmetry laws can be derived relating fluctuations within heterogeneous systems. These statements govern the possible energy transfers that can occur within nonequilibrium systems. In contrast with thermal fluctuations, multiscale fluctuations are linked with cooperative events and therefore may not obey detailed balance. Nonstationary fluctuations occur when there are net energy transfers within a system. We consider droplet coalescence as a clear example of a nonequilibrium system where multiple crossover times are present. In contrast with a thermodynamic cycle, droplet coalescence is nonstationary based on the fact that entropy production occurs. Considering coalescence along with immiscible displacement in porous media, we show that capillary fluctuations can be predicted by a simple scaling law, $\log_{10} S_p \sim \alpha F^p$, with $\alpha = -15$ and $p = 1/2$ matching the fluctuation spectrum in both cases. Multiscale fluctuations are extensible to other systems where gradients in composition, chemical potential, and other intensive variables are operative at a scale that is smaller than the scale of interest. Classes of nonergodic behavior that are defined by macroscopically slow physics are particularly relevant. The formulation is based on classical thermodynamic theory and defines fluctuations in terms of standard quantities that are straightforward to measure in a practical setting.

ACKNOWLEDGMENTS

An award of computer time was provided by the Department of Energy Summit Early Science program. This research also used resources of the Oak Ridge Leadership Computing Facility, which is a U.S. Department of Energy Office of Science User Facility supported under Contract No. DE-AC05-00OR22725. μ CT was performed on the TOMCAT beam line at the Swiss Light Source, Paul Scherrer Institut, Villigen, Switzerland. We are grateful to G. Mikuljan at the Swiss Light Source, whose outstanding efforts have made these experiments possible.

[1] W. Parry, *Topics in Ergodic Theory*, Cambridge Tracts in Mathematics (Cambridge University Press, Cambridge, 2004).

[2] J. v. Neumann, *Proc. Natl. Acad. Sci. USA* **18**, 70 (1932).

- [3] G. D. Birkhoff, *Proc. Natl. Acad. Sci. USA* **17**, 656 (1931).
- [4] R. G. Palmer, *Adv. Phys.* **31**, 669 (1982).
- [5] A. V. Weigel, B. Simon, M. M. Tamkun, and D. Krapf, *Proc. Natl. Acad. Sci. USA* **108**, 6438 (2011).
- [6] M. Schwarzl, A. Godec, and R. Metzler, *Sci. Rep.* **7**, 3878 (2017).
- [7] F. S. Gnesotto, F. Mura, J. Gladrow, and C. P. Broedersz, *Rep. Prog. Phys.* **81**, 066601 (2018).
- [8] P. G. Debenedetti and F. H. Stillinger, *Nature* **410**, 259 (2001).
- [9] A. Crisanti and F. Ritort, *J. Phys. A: Math. Gen.* **36**, R181 (2003).
- [10] G. Tarjus, S. A. Kivelson, Z. Nussinov, and P. Viot, *J. Phys.: Condens. Matter* **17**, R1143 (2005).
- [11] S. S. Datta, H. Chiang, T. S. Ramakrishnan, and D. A. Weitz, *Phys. Rev. Lett.* **111**, 064501 (2013).
- [12] V. D. Borman and A. A. Belogorlov, V. A. Byrkin, and V. N. Tronin, *Phys. Rev. E* **88**, 052116 (2013).
- [13] D. Crandall, G. Ahmadi, M. Ferer, and D. H. Smith, *Physica A: Stat. Mech. App.* **388**, 574 (2009).
- [14] E. Kierlik, P. A. Monson, M. L. Rosinberg, L. Sarkisov, and G. Tarjus, *Phys. Rev. Lett.* **87**, 055701 (2001).
- [15] M. Winkler, M. Gjennestad, D. Bedeaux, S. Kjelstrup, R. Cabriolu, and A. Hansen, *Front. Phys.* **8**, 60 (2020).
- [16] M. Iwamatsu, *J. Chem. Phys.* **134**, 164508 (2011).
- [17] A. Baule, F. Morone, H. J. Herrmann, and H. A. Makse, *Rev. Mod. Phys.* **90**, 015006 (2018).
- [18] H. J. Herrmann and S. Luding, *Continuum Mech. Thermodyn.* **10**, 189 (1998).
- [19] A. Mehta, G. C. Barker, and J. M. Luck, *Proc. Natl. Acad. Sci. USA* **105**, 8244 (2008).
- [20] L. Atia, D. Bi, Y. Sharma, J. A. Mitchel, B. Gweon, S. A. Koehler, S. J. DeCamp, B. Lan, J. H. Kim, R. Hirsch, A. F. Pegoraro, K. H. Lee, J. R. Starr, D. A. Weitz, A. C. Martin, J.-A. Park, J. P. Butler, and J. J. Fredberg, *Nat. Phys.* **14**, 613 (2018).
- [21] H. B. Callen and T. A. Welton, *Phys. Rev.* **83**, 34 (1951).
- [22] R. Kubo, *J. Phys. Soc. Jpn.* **12**, 570 (1957).
- [23] J. Prost, J.-F. Joanny, and J. M. R. Parrondo, *Phys. Rev. Lett.* **103**, 090601 (2009).
- [24] C. Maes, *Phys. Rev. Lett.* **125**, 208001 (2020).
- [25] D. H. Wolpert, *Phys. Rev. Lett.* **125**, 200602 (2020).
- [26] N. R. Morrow, *Indust. Eng. Chem.* **62**, 32 (1970).
- [27] R. T. Armstrong and S. Berg, *Phys. Rev. E* **88**, 043010 (2013).
- [28] S. Berg, H. Ott, S. A. Klapp, A. Schwing, R. Neiteler, N. Brussee, A. Makurat, L. Leu, F. Enzmann, J. Schwarz, M. Kersten, S. Irvine, and M. Stampanoni, *Proc. Natl. Acad. Sci. USA* **110**, 3755 (2013).
- [29] R. T. Armstrong, H. Ott, A. Georgiadis, M. Rücker, A. Schwing, and S. Berg, *Water Resour. Res.* **50**, 9162 (2014).
- [30] L. Cueto-Felgueroso and R. Juanes, *Geophys. Res. Lett.* **43**, 1615 (2015).
- [31] S. M. Hassanizadeh and W. G. Gray, *Adv. Water Res.* **16**, 53 (1993).
- [32] J. Bear and J. J. Nitao, *Transp. Porous Med.* **18**, 151 (1995).
- [33] C. Marle, *Multiphase Flow in Porous Media*, Editions Technip (Institut francais du petrole publications, Paris, 1981).
- [34] S. A. Aryana and A. R. Kovscek, *Transp. Porous Med.* **97**, 373 (2013).
- [35] B. K. Primkulov, A. A. Pahlavan, X. Fu, B. Zhao, C. W. MacMinn, and R. Juanes, *J. Fluid Mech.* **875**, R4 (2019).
- [36] A. A. Pahlavan, H. A. Stone, G. H. McKinley, and R. Juanes, *Proc. Natl. Acad. Sci. USA* **116**, 13780 (2019).
- [37] H. B. Callen, *Thermodynamics* (John Wiley & Sons; 1st edition, New York, 1960).
- [38] M. Grmela and H. C. Öttinger, *Phys. Rev. E* **56**, 6620 (1997).
- [39] H. C. Öttinger and M. Grmela, *Phys. Rev. E* **56**, 6633 (1997).
- [40] D. Froemberg and E. Barkai, *Phys. Rev. E* **88**, 024101 (2013).
- [41] W. G. Gray and C. T. Miller, *Introduction to the Thermodynamically Constrained Averaging Theory for Porous Medium Systems* (Springer, Zürich, 2014).
- [42] S. R. De Groot and P. Mazur, *Non-Equilibrium Thermodynamics* (Dover, Mineola, NY, 2013).
- [43] J. C. Maxwell, *Theory of Heat*, Cambridge Library Collection - Physical Sciences (Cambridge University Press, Cambridge, 2011).
- [44] The Sorting Demon of Maxwell, *Nature* **20**, 126 (1879) .
- [45] A. Ben-Naim, *A Farewell to Entropy* (World Scientific, Singapore, 2008).
- [46] O. Sackur, *Ann. Phys.* **341**, 958 (1911).
- [47] H. Tetrode, *Ann. Phys.* **343**, 434 (1912).
- [48] J. Earman and J. D. Norton, *Stud. Hist. Philos. Sci. Part B: Stud. Hist. Philos. Mod. Phys.* **30**, 1 (1999).
- [49] See Supplemental Material at <http://link.aps.org/supplemental/10.1103/PhysRevE.104.035106> for implementation details pertaining to the Maxwell demon example.
- [50] E. Noether, *Gott. Nachr.* **235**, 405 (1918).
- [51] E. Noether, *Transp. Theory Stat. Phys.* **1**, 186 (1971).
- [52] N. Shiraishi and T. Sagawa, *Phys. Rev. E* **91**, 012130 (2015).
- [53] N. Rupprecht and D. C. Vural, *Phys. Rev. Lett.* **123**, 080603 (2019).
- [54] N. Rupprecht and D. C. Vural, *Phys. Rev. E* **102**, 062145 (2020).
- [55] J. V. Koski, V. F. Maisi, T. Sagawa, and J. P. Pekola, *Phys. Rev. Lett.* **113**, 030601 (2014).
- [56] H. Touchette and S. Lloyd, *Phys. Rev. Lett.* **84**, 1156 (2000).
- [57] T. Sagawa and M. Ueda, *Phys. Rev. Lett.* **104**, 090602 (2010).
- [58] L. Onsager, *Phys. Rev.* **37**, 405 (1931).
- [59] J. Xu, S. Kjelstrup, D. Bedeaux, A. Røsørde, and L. Rekvig, *J. Colloid Interface Sci.* **299**, 452 (2006).
- [60] I. Battiato, D. M. Tartakovsky, *J. Contam. Hydrol.* **120–121**, 18 (2011).
- [61] I. Battiato, D. M. Tartakovsky, A. M. Tartakovsky, and T. Scheibe, *Adv. Water Resour.* **32**, 1664 (2009).
- [62] J. H. Cushman and D. O'Malley, *J. Hydrol.* **531**, 161 (2015).
- [63] J. H. Cushman and T. R. Ginn, *Transp. Porous Media* **13**, 123 (1993).
- [64] J. D. Paulsen, R. Carmigniani, A. Kannan, J. C. Burton, and S. R. Nagel, *Nat. Commun.* **5**, 3182 (2014).
- [65] D. G. A. L. Aarts, H. N. W. Lekkerkerker, H. Guo, G. H. Wegdam, and D. Bonn, *Phys. Rev. Lett.* **95**, 164503 (2005).
- [66] W. D. Ristenpart, P. M. McCalla, R. V. Roy, and H. A. Stone, *Phys. Rev. Lett.* **97**, 064501 (2006).
- [67] M. Wu, *Phys. Fluids*. **16**, L51 (2004).
- [68] M. Orme, *Prog. Energy Combust. Sci.* **23**, 65 (1997).
- [69] S. C. Case and S. R. Nagel, *Phys. Rev. Lett.* **100**, 084503 (2008).
- [70] J. D. Paulsen, J. C. Burton, and S. R. Nagel, *Phys. Rev. Lett.* **106**, 114501 (2011).

- [71] J. D. Paulsen, J. C. Burton, S. R. Nagel, S. Appathurai, M. T. Harris, and O. A. Basaran, *Proc. Natl. Acad. Sci. USA* **109**, 6859 (2012).
- [72] S. Perumanath, M. K. Borg, M. V. Chubynsky, J. E. Sprittles, and J. M. Reese, *Phys. Rev. Lett.* **122**, 104501 (2019).
- [73] J. E. McClure, Z. Li, M. Berrill, and T. Ramstad, [arXiv:2007.12266](https://arxiv.org/abs/2007.12266).
- [74] M. B. Weissman, *Rev. Mod. Phys.* **60**, 537 (1988).
- [75] W. S. Kendal, *Physica A* **421**, 141 (2015).
- [76] P. Bak, C. Tang, and K. Wiesenfeld, *Phys. Rev. Lett.* **59**, 381 (1987).
- [77] F. Alpak, I. Zacharoudiou, S. Berg, J. Dietderich, and N. Saxena, *Comput. Geosci.* **23**, 849 (2019).